nature communications

Article

https://doi.org/10.1038/s41467-024-55802-w

Coeval upper crustal extension and surface uplift in the Central Taurides (Türkiye) above the Cyprus Subduction Zone

Received: 20 March 2024

Accepted: 30 December 2024

Published online: 25 April 2025

Check for updates

Tunahan Aykut[1] ✉, Cengiz Yıldırım[1], I. Tonguç Uysal[2,3] ✉, Uwe Ring[4] & Jian-xin Zhao[3]

The Central Taurides represent a high-relief topography with a multi-phase uplift history linked to mantle-driven, deep-seated processes. While the uplift history is well constrained, the temporal relationship between surface uplift and brittle surface deformation is poorly documented. Here, we combine U-Th geochronology, microstructural analysis, and fault-slip data to decipher the timing and mechanism of upper crustal deformation above the Cyprus Subduction Zone, which has experienced 1.5 km of surface uplift since 450 ka. Kinematic measurements indicate widespread normal faulting due to NE-SW horizontal tension in the upper crust. U-Th ages of fault-related calcites show continuous faulting from the Middle/Late Pleistocene to the Holocene, with a conspicuous clustering at circa 450 ka. Our study emphasizes the connection/coupling between deep-seated and surface processes. It suggests that extensional deformation and rapid surface uplift may occur concurrently, creating relief-bounding normal fault zones and high-relief dynamic landscapes on a short timescale in the overriding plates.

The deep-seated processes may lead to abrupt changes in surface elevations, reorganization in landscape dynamics (e.g., topographical relief), and styles of deformation (Faccenna et al.[1]; Schildgen et al.[2]). However, deciphering the spatiotemporal relationship between deep-seated processes (e.g. slab tearing/breakoff, asthenospheric upwelling) and upper crustal deformation (e.g. faulting) is challenging, as there are little geochronological constraints, especially at erosional margins of orogenic plateaus, where syn-tectonic sediments have been largely obliterated. The southern margin of the Central Anatolian Plateau (CAP) represents a unique region to study this connection, where the relationship between regional surface uplift and mantle-driven processes, such as slab tearing/break-off and asthenospheric upwelling have been proposed. This argument is based on the remarkable uplift of 2 km along the margin, which occurs without horizontal shortening, as shown by horizontal layers of the Tortonian marine deposits at 2000 m above sea level (Mutlu and Karabulut[3]; Biryol et al.[4]; Cosentino et al.[5]; Schildgen et al.[6,7,2]; Öğretmen et al.[8]; Portner et al.[9]; Racano et al.[10,11]; Aykut et al.[12]) (Fig. 1a, b). However, despite the pronounced topographic expression of the faults at the southern margin of the CAP, the link between deep-seated processes, upper crustal brittle deformation, and surface uplift remains to be investigated.

The southern margin of the CAP is situated in the upper plate north of the Cyprus Subduction Zone, where the African Plate subducts beneath the Anatolian Plate (Fig. 1a). The convergence between the African, Arabian and Eurasian Plates has dominated the geological evolution of the Eastern Mediterranean since the Mesozoic (Jolivet and Faccenna[13]; Schattner[14]). The subduction of the African Plate under Anatolia is accommodated along two active plate boundaries: The Hellenic and Cyprus trenches. Along these trenches, the subducting slabs include the north-dipping Cyprus slab and the ENE-dipping Antalya slab, which are currently separated by an upper mantle slab

[1]Eurasia Institute of Earth Sciences, Istanbul Technical University, Istanbul, Türkiye. [2]Istanbul University-Cerrahpaşa, Department of Geological Engineering, Istanbul, Türkiye. [3]School of the Environment, The University of Queensland, Brisbane, QLD, Australia. [4]Department of Geological Sciences, Stockholm University, Stockholm, Sweden. ✉e-mail: aykut20@itu.edu.tr; t.uysal@uq.edu.au

https://doi.org/10.1038/s41467-024-55802-w

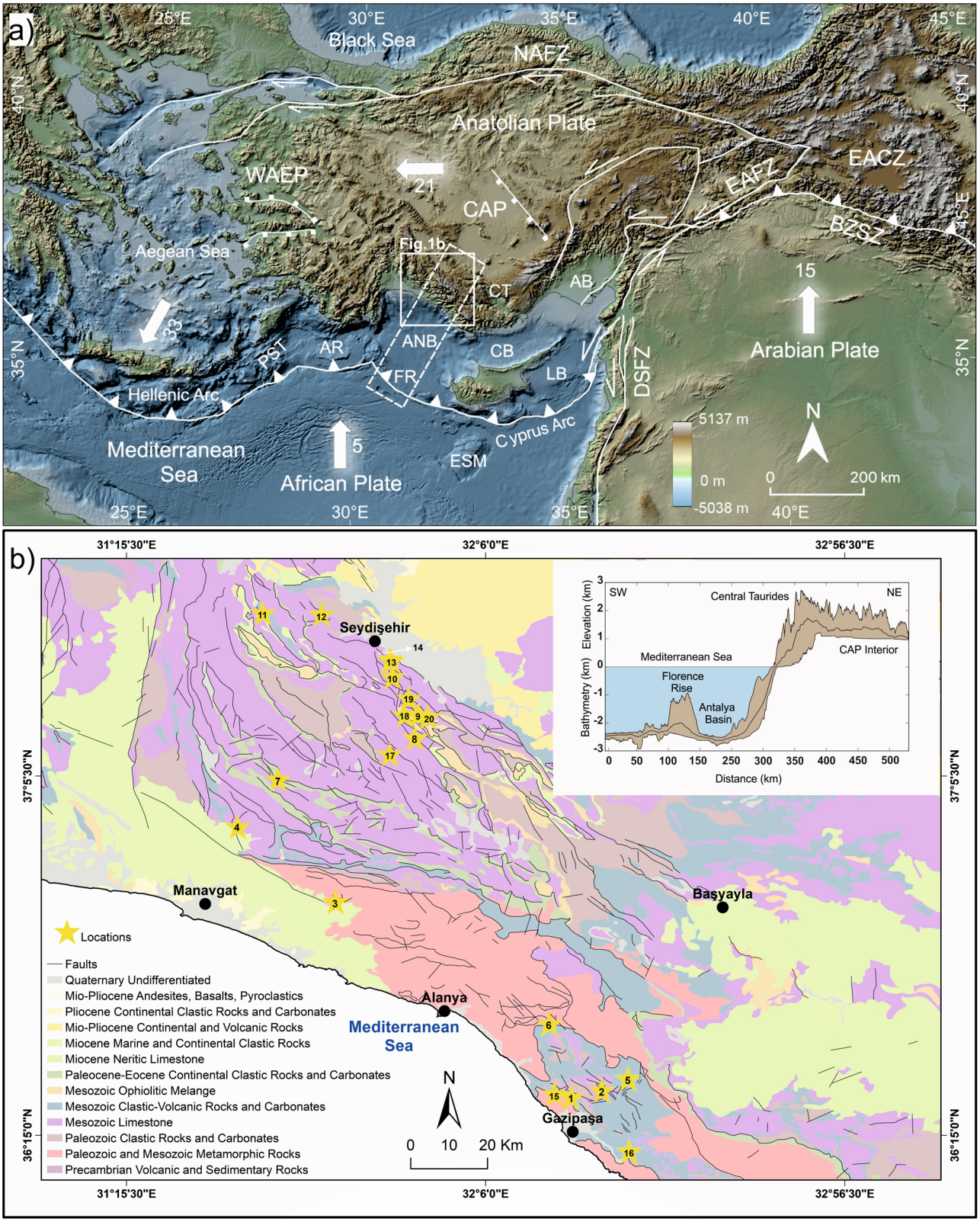

Fig. 1 | Tectonic and geological framework of the study area. a Simplified active tectonic map of the Eastern Mediterranean and Anatolia. The white box indicates the study area. White arrows denote the movement directions relative to Eurasia. GPS velocities (mm/yr) (white numbers next to arrows) are from Reilinger et al.[16]. The white rectangle with dashed lines represents the footprint of the swath profile shown in (**b**). The digital elevation model and bathymetry data are obtained from GTOPO30 data (https://www.usgs.gov/centers/eros/science/usgs-eros-archive-digital-elevation-global-30-arc-second-elevation-gtopo30). WAEP: Western Anatolian Extensional Province, EACZ: Eastern Anatolian Contractional Province, BZSZ: Bitlis-Zagros Suture Zone, NAFZ: North Anatolian Fault Zone, EAFZ: East Anatolian Fault Zone, DSFZ: Dead Sea Fault Zone, PST: Pliny and Strabo Trenches, AR: Anaximander Mountains, FR: Florence Rise, ANB: Antalya Basin, CB: Cilicia Basin, LB: Levant Basin, AB: Adana Basin, LT: Latakia Basin, CT: Central Taurides, CAP: Central Anatolian Plateau, ESM: Eratosthenes Seamount. **b**. General geological features of the study area. Faults are from Şenel, ([31]). Swath profile presented as an inset.

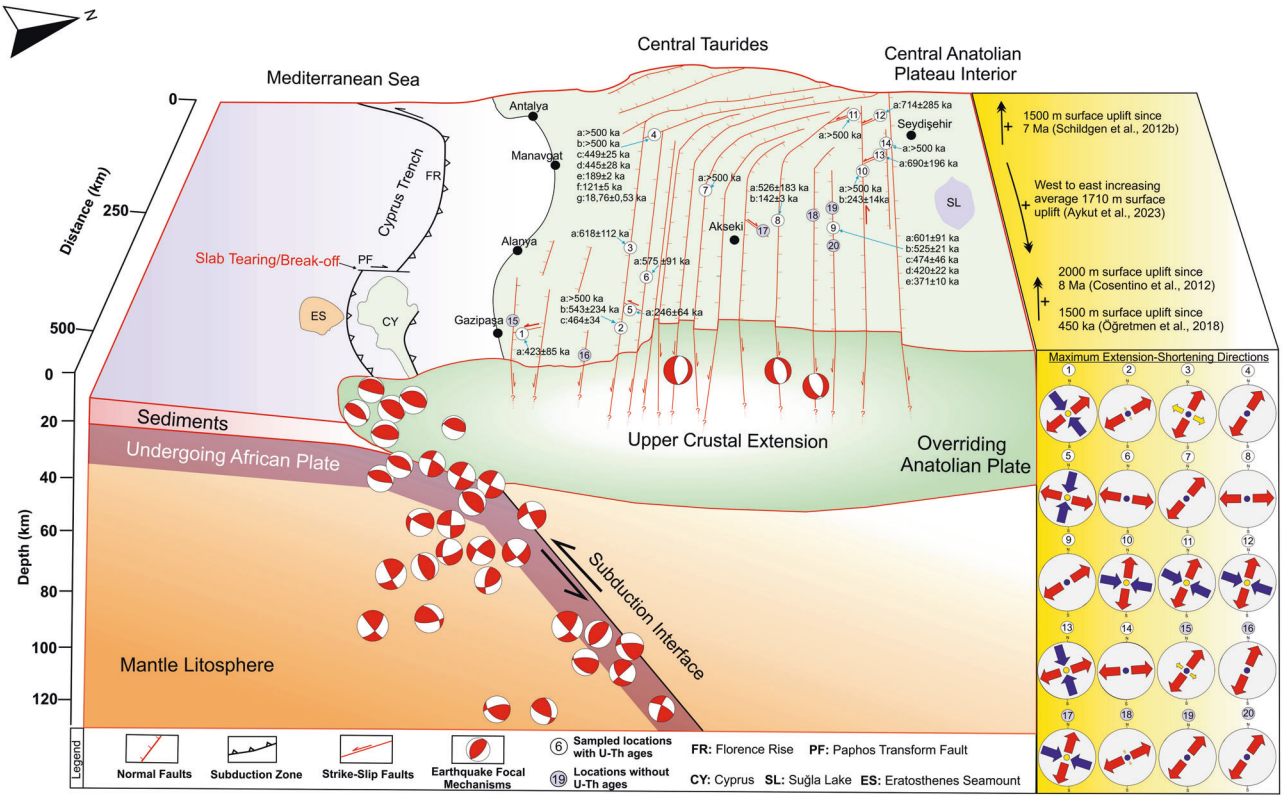

Fig. 2 | Illustrative representation of Cyprus Subduction Zone and Central Taurides. Sampling locations within the Central Taurides are shown with corresponding U-Th ages with associated errors. Maximum extension (red arrows) and shortening (blue arrows) directions are given in the lower right corner (Supplementary Figs. S1–S15). Earthquake focal mechanisms along the subduction interface and within the overriding Anatolian Plate are from Boğaziçi University Kandilli Observatory and Earthquake Research Institute (KOERI) (http://www.koeri.boun.edu.tr/sismo/2/moment-tensor-solutions/), Disaster and Emergency Management of Turkey (AFAD) (https://deprem.afad.gov.tr/faycozumleri?lang=en), Wdowinski et al.[19]; Imprescia et al.[20]; Howell et al.[17] and Güvercin et al.[18]. Crustal thicknesses are derived from Tezel et al.[68]. The surface uplift estimates in the yellow box are for the Central Taurides. Note that the fault network is generalized.

gap (Biryol et al.[4]; Mutlu and Karabulut[3]; Portner et al.[9]). Segmentation of these slabs, and associated mantle flow, may have contributed to the <8 Ma uplift of the Central Anatolian Plateau (Schildgen et al.[2]). Further west, the relationship between slab retreat, southward migration of the magmatic arc and lithospheric extension (e.g. normal faulting) in the Aegean Sea (i.e. the Hellenic Arc) transect is well-constrained (Ring et al.[15]). However, the relationship between deep-rooted processes and surface faulting, particularly above the Cyprus Subduction Zone, has remained equivocal due to the lack of isotopic age data.

The Cyprus Subduction Zone is an active plate boundary where the African and Anatolian plates converge at rates of ~5–15 mm/yr (Reilinger et al.[16]). The subduction zone extends from the Hellenic Arc south of Crete to the east, crosses southern Cyprus with an arcuate shape and merges with the Arabian Plate through a left-lateral strike-slip deformation (Fig. 1a). It extends over a large area with subdivided deformation zones rather than a uniform sharp plate boundary.

The dynamic tectonic history of the region has caused a complex subduction-collision system including deep marine basins (e.g., Antalya, Levant, Adana, Latakia, Cilicia Basins), bathymetric highs (e.g. Florence Rise, Anaximander Mountains, Eratosthenes Seamount) and major fault zones (e.g. Pliny and Strabo Faults, Paphos Transform Fault) (Fig. 1a) (Howell et al.[17]). To the west, the boundary between the Hellenic and Cyprus trenches is controlled by the NE-SW striking Pliny and Strabo shear zones. South of the Antalya Basin, the surface projection of the subduction zone turns in an NW-SE orientation (Howell et al.[17]; Güvercin et al.[18]). Here, the Pliny and Strabo shear zones merge with the bathymetric high of the Florence Rise (Fig. 1a). This rise consists of strongly deformed and elevated oceanic sediments that bury the subduction interface under a thick sedimentary cover (>10 km). Structural studies and earthquake focal mechanisms (Wdowinski et al.[19]; Imprescia et al.[20]; Howell et al.[17]; Güvercin et al.[18]) provide evidence of ongoing convergence along the Florence Rise. Further to the east, the subduction can be traced along the south of Cyprus, where the Eratosthenes Seamount has formed the collision zone in the latest Pliocene (Robertson[21]; Schattner[14]; Ring and Pantazides[22]). Tomographic imaging suggests no slab from eastern Cyprus to the Levant mainland (Biryol et al.[4]; Portner et al.[9]). The absence of a slab was related to the lateral migration of the slab break-off (11–8 Ma ago), which propagated from the Bitlis Suture Zone (Keskin[23]; Şengör et al.[24]) towards eastern Cyprus (Faccenna et al.[1]; Schildgen et al.[2]). The eastern extension of the Cyprian Arc is more transpressional with a left-lateral component, characterised by wrench tectonics based on kinematic, seismic and bathymetric evidence (Wdowinski et al.[19]; Kinnaird and Robertson[25]). The arrival of the Eratosthenes Seamount is thought to have locked the central segment of the Cyprus subduction zone (Robertson[21]; Schattner[14]; Kinnaird and Robertson[25]). As a consequence, the dextral Paphos Transform Fault formed and segmented the subducting slab into the Western Cyprus Slab (or Antalya Slab) and the Eastern Cyprus Slab which merges into the transpressional, slab-free plate boundary in the east (Biryol et al.[4]; Portner et al.[9]; Güvercin et al.[18]) (Fig. 2).

The stress fields, rheologies and deformation mechanisms of the downgoing African Plate, the overriding Anatolian Plate and the subduction interface along the Cyprus Trench have long been debated (Wdowinski et al.[19]; Schildgen et al.[7]; Howell et al.[17]; Güvercin et al.[18]; Aykut et al.[12]). Due to limited seismic activity, the subduction interface is assumed to deform aseismically with low elastic-strain accumulation (Vernant et al.[26]; Howell et al.[17]). Reverse and strike-slip

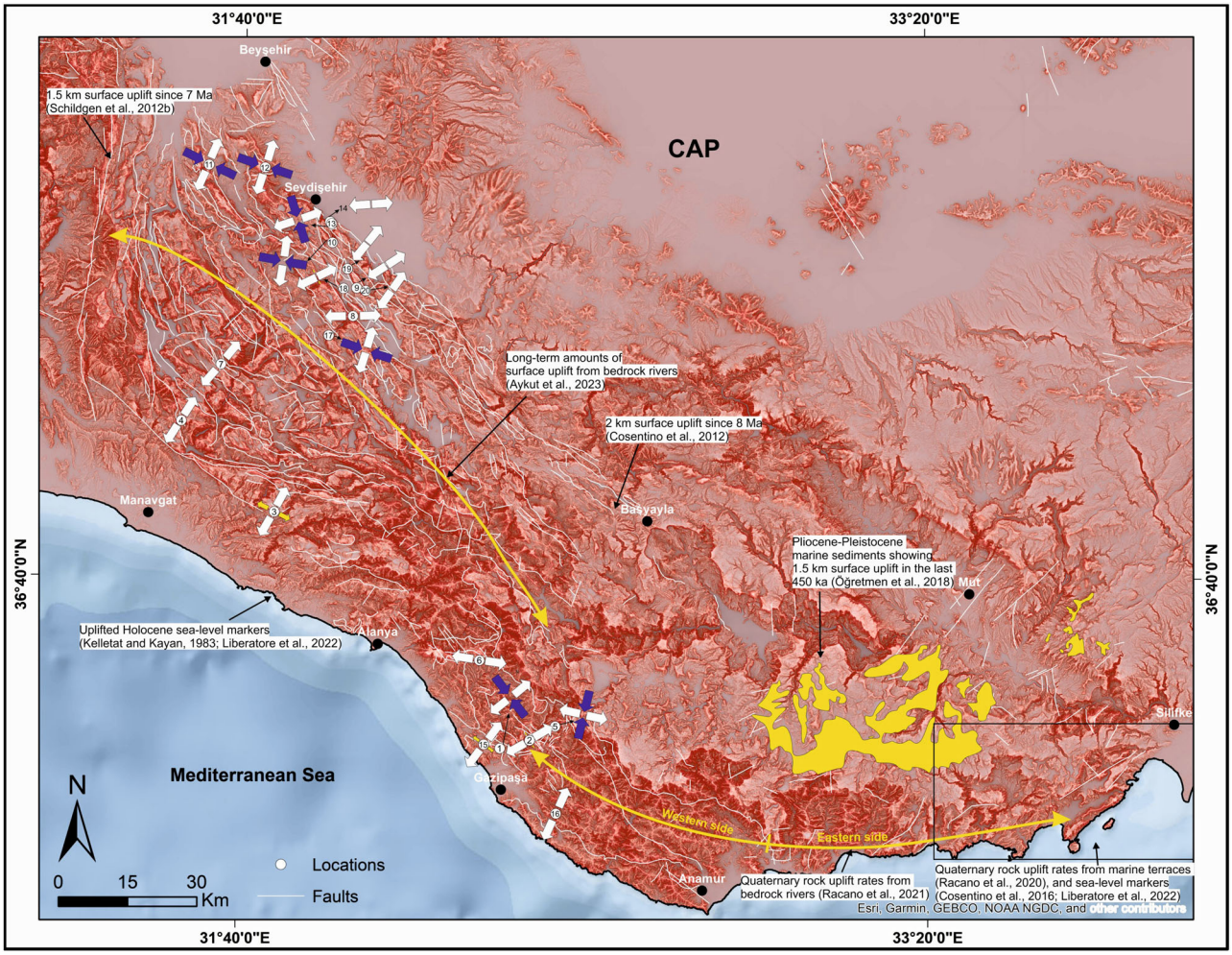

Fig. 3 | Red-relief image map (Chiba et al.[69]) illustrating the topography across the Central Taurides. Spatial distribution of uplift constraints from previous studies is depicted in the figure. Yellow polygons represent Pliocene-Pleistocene marine sediments from Öğretmen et al.[8] White and blue arrows are maximum extension/shortening directions respectively, based on our kinematic analysis (Fig. 2, Supplementary Figs. S1–S15). The white lines indicate faults (Şenel et al.[31]). CAP: Central Anatolian Plateau.

earthquake focal mechanisms from depths >40 km provide evidence of contractional and deep brittle deformation (Howell et al.[17]; Güvercin et al.[18]).

Active brittle deformation of the overriding Anatolian Plate (southern part) has been associated with tensional horizontal stress (Monod et al.[27]; Imprescia et al.[20]; Schildgen et al.[7]; Howell et al.[17]; Aykut et al.[12]). Slow seismic velocities beneath southern Anatolia have been interpreted as an expression of a slab tear causing an upwelling of the asthenosphere and associated surface uplift (Faccenna et al.[1]; Biryol et al.[4]; Mutlu & Karabulut,[3]; Schildgen et al.[2]; Portner et al.[9]). Biostratigraphic evidence suggests 2 km of surface uplift since 8 Ma (Cosentino et al.[5]; Schildgen et al.[6,2]). Recent studies found that 1.5 km of this surface uplift has occurred in the last 450 ka (at rates of 3.21–3.42 mm/yr) (Öğretmen et al.[8]), which is consistent with the accelerated surface uplift during the last 1.6 Ma (Schildgen et al.[2]). Morpho-tectonic markers such as Quaternary tectono-karstic depressions, deep bedrock river incision (more than 1500 m), characteristic wind gaps, exposed fault planes, prevalent low-relief perched upland surfaces (above 2000 m), uplifted wave-cut notches, marine terraces and major slope-break knickzones have enabled further quantification of the uplift history (Kelletat and Kayan[28]; Monod et al.[27]; Schildgen et al.[6,7]; Cosentino et al.[29]; Racano et al.[10,11]; Liberatore et al.[30]; Aykut et al.[12]) (Fig. 3). Uplifted wave-cut notches, beachrocks and algae fossils revealed 0.5–1.3 m cumulative uplift at rates of 0.9–2 mm/yr throughout the Holocene (Kelletat and Kayan,[28]; Cosentino et al.[29]; Liberatore et al.[30]). Marine-terrace and bedrock river modelling studies yielded 1.1–6.3 mm/yr rock uplift rates in the Late Quaternary (Racano et al.[10,11]) (Fig. 3).

The upper crust of the Cyprus Subduction Zone between the Central Anatolian Plateau (Seydişehir) and the Mediterranean Sea (Gazipaşa) presents a series of NW-SE striking fault zones (mostly within Mesozoic limestones) (Şenel, 2002[31]) that have prominent topographical expressions at the highly erosional and karstified orogenic plateau margin (Fig. 1b). Despite the active convergence and the significant impact of mantle-rooted and crustal processes throughout the region (Faccenna et al.[1]; Biryol et al.[4]; Schildgen et al.[2]; Racano et al.[11]; McPhee et al.[32]; Aykut et al.[12]), the Quaternary faulting history and its seismic hazard potential remains unknown. The erosional nature of the landscape and a dearth of fault-related stratigraphic and sedimentological markers along and within the overriding plate make it difficult to decipher the timing of brittle deformation. U-series dating of syn-tectonic calcites can have important implications for the evolution of erosional landscapes (Uysal et al.[33–35]; Nuriel et al.[36,37]; Karabacak et al.[38]).

In this study, we investigate relief-bounding faults in a 200 km long section running from southwest to northeast from the Mediterranean coast to the Central Anatolian Plateau (CAP) interior, respectively, across the overriding Anatolian Plate (southern part,

between Seydişehir and Gazipaşa) (Figs. 1–3). We implement U-series (U-Th) geochronology of syn-tectonic calcites in combination with microstructural and kinematic analyses at the southern margin of the CAP. We present U-Th age data of Quaternary brittle deformation across the orogenic plateau margin and show the spatiotemporal deformation patterns above this complex subduction zone in the Eastern Mediterranean. Our data show a significant temporal correlation between regional surface uplift and normal faulting, suggesting a strong spatial connection and temporal overlap between upper crustal deformation (i.e. normal faulting) and mantle-driven processes along the southern margin of the CAP.

Results

We present field and microstructural observations from major fault zones and U-series dating of faulting-related calcites to constrain the Quaternary brittle deformation history of the overriding plate. The methods used and the data are detailed in the supplementary material.

Kinematics of the overriding plate deformation

Our field measurements focused on the youngest faulting phase, revealing the active deformation mechanism of the upper plate. The results provide the directions of the stress tensor and the stress ratios (R) of the principal stress axes (σ1, σ2, and σ3). Major faults are up to 150 km long, segmented, NW-SE striking normal fault zones (Fig. 2). Seismicity along these faults is high, as shown by earthquake data (Aykut et al.[12]), and the earthquake focal mechanism solutions indicate normal faulting in the upper crust (<10 km) (Fig. 2). Vertical to subvertical calcite slicken-lines and slicken-fibres (Figs. 4, 5) show that most faults have dip-slip components (Fig. 5 and Supplementary Figs. S1–S15). NW-SE striking strike-slip faulting is also evident in some locations (Location 10, Figure S10). Based on cross-cutting relationships and fault geometries, we have also identified extension-parallel, NE-SW and N-S striking secondary fault zones merging with NW-SE oriented first-order normal fault zones at low angles. Paleo-stress analyses yielded NE-SW horizontal tension for the primary (large) normal fault zones, whereas NW-SE compressional and NE-SW tensional stress directions were determined for the small strike-slip faults (Fig. 2, Figures S1a, S4, S5, S11, S12-a, Supplementary Table S1). Following the geomorphic analyses and field observations presented in Aykut et al.[12], we implemented U-Th dating exclusively on those faults with proven neotectonic activity.

Microstructural evidence

Analyses with the optical thin section microscope and the scanning electron microscope (SEM) show that the microstructures of calcite mainly have the appearance of blocky crystals. These coarse-grained, blocky calcites often exhibit twinning (Fig. 4e, g, h, f, i, l), indicating significant deformation caused by faulting (Nuriel et al.[37]; Karabacak et al.[38]). The samples examined contain randomly distributed calcite fragments, brecciated zones, calcite gouges, slickenlines, slickenfibres, fault grooves, microfractures and displaced dilation veins (Fig. 4). Large and small calcite crystals in the micritic limestone matrix (fault gouge) are interpreted as brecciated zones (Fig. 4h, k). Some of these gouges make sharp contacts with relatively homogeneous crystalline zones (Fig. 4h–k). SEM analyses of fault-related calcites show pronounced slickensides, slickenfibers, pits and grooves (Fig. 4a–d). SEM and optical microscope images of samples from locations 4-g (Fig. 4c) and 8-b (Fig. 4j) show distinct striations of calcite coatings on the fault planes, indicating syn-tectonic formation (cf., Oren et al.[39]; Karabacak et al.[38] and references therein).

U-Th geochronology

U-series dating of fault-related carbonates (calcite fibres, striated calcites and striated calcite coatings) yielded twenty-one U-Th ages ranging between 714 ± 285 ka (or >500 ka, which is indistinguishable from ^{238}U-^{234}U-^{230}Th secular equilibrium) and 18.76 ± 0.53 ka (Fig. 2, Supplementary Table S2). The U-Th ages of syn-tectonic slickenfibres and striated calcites on normal and strike-slip faults vary from 618 ± 112 ka (or >500 ka) to 121 ± 5 ka and from 714 ± 285 ka (or >500 ka) to 243 ± 14 ka, respectively (Table S2). Additionally, seven samples gave secular equilibrium ages (>500 ka). However, most U-Th ages cluster around 450 ka (Fig. 6). Carbonate coatings on the normal fault planes (sample b from location 8 and sample g from location 4, Fig. 2) yielded U-Th ages of 142 ± 3 ka and 18.76 ± 0.53 ka (Fig. 6). In general, the U-Th ages of brittle extensional structures show a continuous normal and strike-slip faulting from the Middle/Late Pleistocene up to the Holocene, with clusters at 450 ka and 100–250 ka period (Fig. 6).

Discussion

Our combined kinematic and U-Th age results, earthquake focal mechanism solutions (Fig. 2) and GPS-derived strain-rate fields (Howell et al.[17]) indicate active NE-SW directed horizontal extension accommodated by NW-SE striking normal fault zones within the upper plate of the Cyprus Subduction Zone. Continuous U-Th ages from multiple generations of fault-related calcites range from >500 ka to 18.76 ± 0.53 ka, providing evidence of normal faulting from the Middle/Late Pleistocene to the present. The brittle deformation ages clustering at 450 ka may indicate that an important geodynamic event caused an acceleration of extensional surface deformation in the Middle Pleistocene. This cluster (Fig. 6) coincides with the starting point of a rapid (3.21–3.42 mm/yr) surface uplift phase that caused an uplift of 1.5 km in the last 450 ka (Öğretmen et al.[8]). The bedrock river inversions reported by Racano et al.[11] also show peak values for rock uplift at 400–450 ka and 150–250 ka, reaching rates of 5.1 mm/yr. Studies on the modelling of marine terraces (Racano et al.[10]) revealed uplift rates ranging between 1.1 and 3.8 mm/yr with decreasing rate patterns from the Late Quaternary (500 ka) to the present. The second significant U-Th age cluster at 100–250 ka (Fig. 6) also overlaps with high uplift rates derived from marine terrace elevations and bedrock river inversions. Thus, the data from geomorphic markers, biostratigraphic indicators and our U-Th geochronology results show that extensional deformation was coeval with vertical deformation (surface uplift) over the last 450 ka (Figs. 6, 7).

Previously, various geodynamic concepts have been invoked to explain the active deformation at the southern margin of the CAP, such as lower crustal flow (Fernandez-Blanco et al.[40]), slab roll-back (Koç et al.[41,42]) and slab deformation and asthenospheric upwelling (Schildgen et al.[6,7,2]; Cosentino et al.[5]; Öğretmen et al.[8]; Racano et al. [10,11]). Some studies have also proposed lithospheric delamination to explain the uplift of the Central and Eastern Anatolian Plateaus, partly including the Central Taurides (Bartol and Govers[43]; Meijers et al. [44]). Our kinematic observations in the upper crust show a lack of active thrust/reverse faulting (i.e. shortening), which is significant despite the rapid surface uplift (Öğretmen et al.[8]), Quaternary rock uplift (Kelletat and Kayan[28]; Racano et al.[10,11]; Liberatore et al.[30]) and dynamic-transient topography (Monod et al.[27]; Schildgen et al.[6]; Aykut et al.[12]). Our quantification of the timing of extensional surface deformation, which provides evidence for contemporaneous surface uplift and normal faulting in the last 450 ka, favours mantle-driven control over upper crustal deformation. Considering the observations of P wave tomography data showing a distinct slab gap and slow velocity anomalies detected beneath southern Türkiye (Faccenna et al. [1]; Biryol et al.[4]; Mutlu & Karabulut[3]; Portner et al.[9]), together with evidence for different extension directions in southern Türkiye (N-S, E-W, NE-SW, NW-SE) (Glover and Robertson [45,46]; Schildgen et al.[7], Howell et al.[17], Aykut et al.[12]) (Fig. 7); it is becoming increasingly plausible that slab deformation and subsequent asthenospheric upwelling are key processes contributing to the ongoing deformation observed in the Central Taurides (Fig. 7). Other mechanisms, such as slab roll-back, folding related to north-south contraction, thermal or viscous crust

https://doi.org/10.1038/s41467-024-55802-w

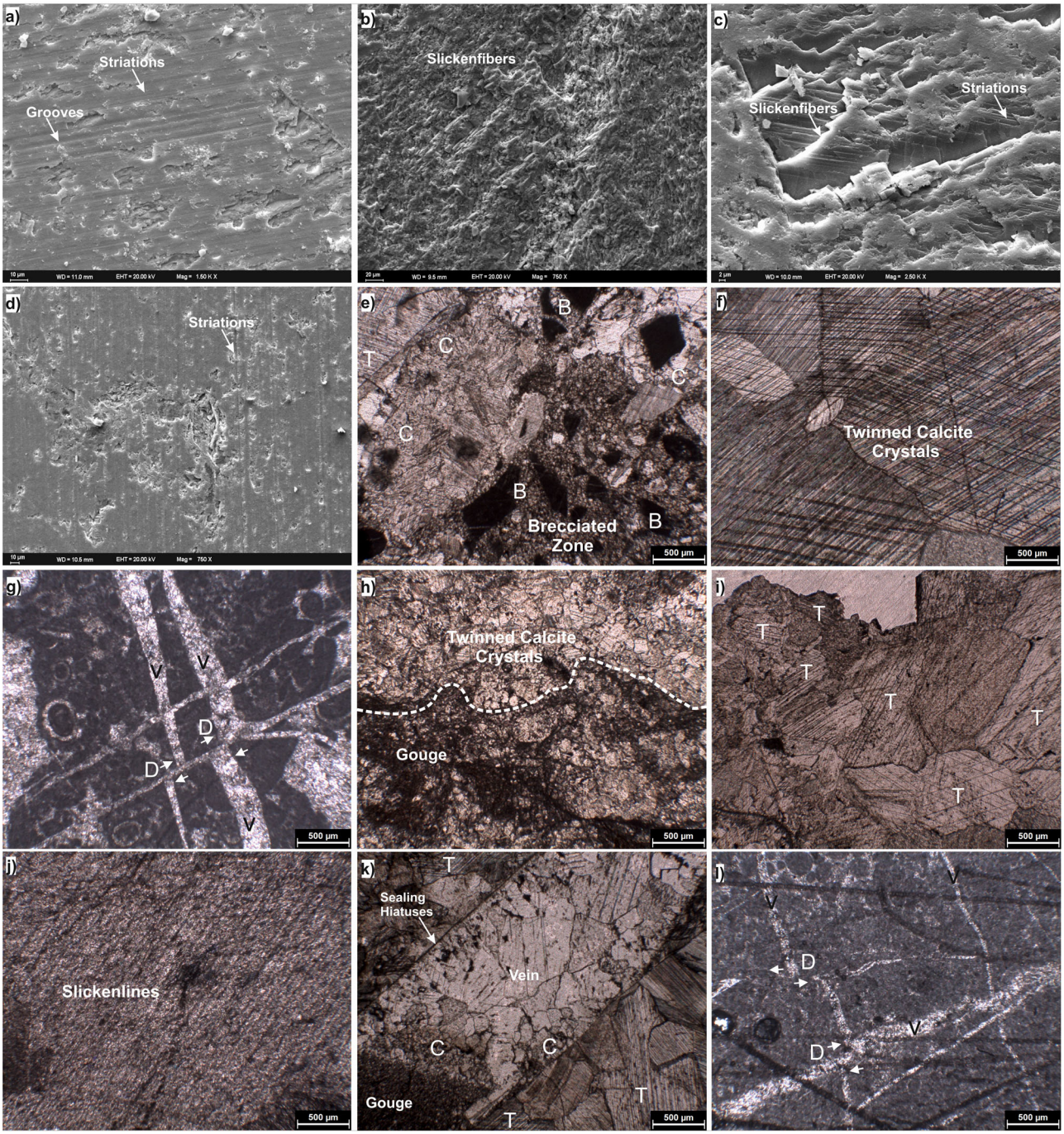

Fig. 4 | Photomicrographs of Fault-Related Calcite Precipitates. Scanning electron microscope (SEM) (**a**–**d**) and optical microscope (**e**–**l**) photomicrographs of fault-related calcite precipitates. **a** Location 4-sample c, **b** Location 8-sample a, **c** Location 4-sample g, **d** Location 9-sample e, **e** Location 12-sample a, **f** Location 12-sample a, **g** Location 8-sample b, **h** Location 4-sample d, **i** Location 9-sample d, **j** Location 8-sample b, **k** Location 13-sample a, **l** Location 8- sample a. B = Breccia, C = Cataclasis, D: Displacement, V = Vein and T = Twining.

deformation, or continental underthrusting, do not appear to explain the rapid surface uplift and concurrent extension observed in the upper crust in a relatively short time (<500 ka).

The majority of the presented U-Th ages are younger than the formation of the Paphos Transform Fault, which is proposed to have formed as a result of the underthrusting of the Eratosthenes Seamount ~2 Ma ago (Robertson[21]; Schattner[14]; Kinnaird and Robertson[25]). We envisage that the underthrusting of the isolated seamount slowed down the subduction beneath the central part of the Cyprus Subduction Zone, leading to differential underthrusting that was accommodated by the formation of the Paphos Transform Fault. The Paphos Fault subsequently caused a tear in the slab (Mutlu and Karabulut[3]; Biryol et al.[4]; Portner et al.[9]) (Fig. 7). Mantle flow through the tear might have controlled the surface uplift after 1.6 Ma in the Central Taurides (Schildgen et al.[6,2]). Ages of ≤450 ka for upper crustal extension, together with accelerating surface uplift rates (Öğretmen et al.[8]) and rock uplift rates (Racano et al.[11]) (Figs. 2, 5) may indicate that the most pronounced phase of surface uplift and the widespread upper-crustal extension lagged behind initial slab deformation by ~1 Ma. Peaking surface deformation in the Middle Pleistocene may also indicate that the slab broke off at circa 450 ka (or shortly before), after the initial tearing event in the Early Pleistocene (Fig. 7). This conclusion is

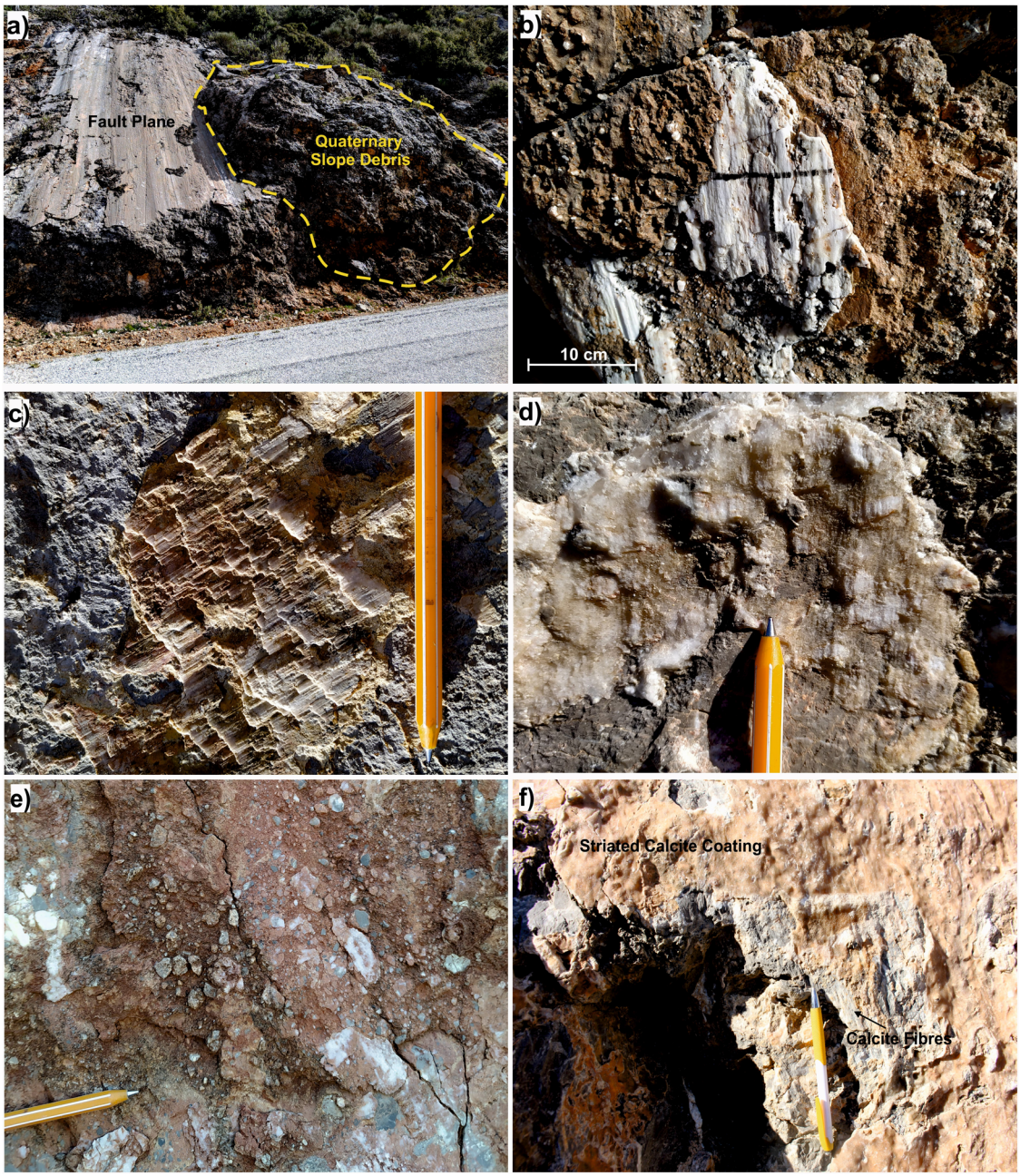

Fig. 5 | Examples of syn-tectonic deformation structures on studied fault planes. a Exposed normal fault plane with overlying amalgamated Quaternary slope debris at location 4. **b** Close up of slicken fibres demonstrating that the Quaternary slope debris has been cut by faults' activity at location 4. Characteristic calcite fibres at location 14 (**c**) and location 9 (**d**). **e** Brecciation on fault plane at location 19. **f** Calcite fibres and striated calcite coatings on normal fault plane at location 8. **a**, **b**, **d** are from Aykut et al.[12]. Note that photos and kinematic features for every location are given in the supplementary file (Figures S1–S15).

consistent with observations from laboratory experiments and numerical models, which predict that mantle upwelling through slab gaps after slab break-off can lead to rapid uplift in time windows as short as 100 ka and to extension in the overriding plates (van Hunen and Allen[47]; Duretz and Gerya[48]; Kiraly et al.[49]). However, to substantiate this interpretation, additional geophysical data and further geochronological constraints are needed to better understand the extent of the impact of geodynamic drivers on the contemporaneous Late Quaternary surface uplift and normal faulting above the Cyprus Trench.

What is the commencement age of the extension? U-Th ages of >500 ka indicate that extensional deformation was also active before the Middle Pleistocene. These U-Th ages may reflect the normal faulting events between ~2 Ma and 500 ka, following the possible slab deformation event around 2 Ma (Robertson[21]; Schattner[14]; Kinnaird and Robertson[25]). >500 ka ages may also represent pre-Quaternary extension, most likely related to the retreat of the Cyprus slab before the collision and slab deformation at the Cyprus Subduction Zone (Koç et al.[50,41]). Pre-Quaternary extension has also been identified in the Aksu Basin, Akşehir Graben, Altınapa Basin, Yalvaç Basin and Manavgat Basin within the Taurides (Çiner et al.[51]; Koç et al.[50,41]; Schildgen et al. [7]). Some of these studies have shown that the upper limit of the extension in the Central Tauride basins extends up to the Middle Miocene (Koç et al.[50,41]). Therefore, our >500 ka U-Th ages may also represent the normal faulting events between the Middle-Miocene and the Quaternary. The unidirectional (NE-SW) extension in our kinematic

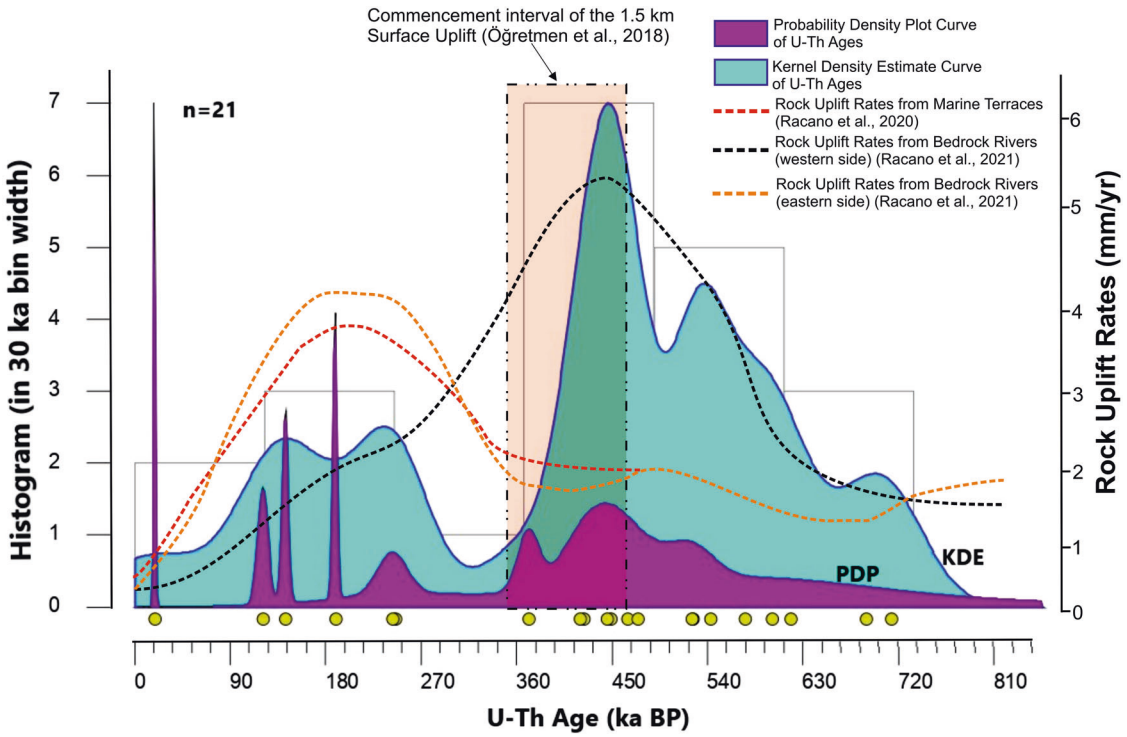

Fig. 6 | Graphical distribution of U-Th ages (DensityPlotter 8.5; Vermeesch[70]), together with the temporal variations in surface and rock uplift values. PDP: Probability Density Plot Curve; KDE: Kernel Density Estimate Curve. Rectangles are sample histograms. Yellow circles present the U-Th ages of the samples in this study. Secular equilibrium U-Th ages (>500 Ka) are excluded. Please note the spatial distribution of the uplift constraints depicted in Fig. 3.

analysis and the coarse topographical texture may reflect the footprints of the NE subducting Antalya Slab's retreat during this period (Biryol et al.[4]; Koç et al.[41,42]; Güvercin et al.[18]; Aykut et al.[12]), especially in the region between Antalya and Alanya. The compensation of active deformation along the NW-SE striking inherited structural zones may also explain the unidirectional NE-SW extension.

Mantle-driven surface uplift and upper crustal extension have been proposed as a viable process above several convergent plate boundaries worldwide (e.g. Apennines (Italy), Tibetan Plateau, Western Alps, SE China, and Central Andes) (D'Agostino et al.[52]; Blisniuk et al.[53]; Faure Walker et al.[54]; Li et al.[54]; Kar et al.[55]; Nocquet et al.[56]). These studies have emphasised the influence of mantle-rooted processes such as slab deformation, mantle upwelling, and various mantle flows on long-wavelength topographic growth and extensional surface deformation. For example, one of the similar places which have a close geographical location and similar climatic, lithological and tectonic setting to Central Taurides, the Apennines above the Calabria Subduction Zone, has been shown to undergo rapid uplift and upper crustal extension as a result of mantle upwelling through slap gaps (D'Agostino et al.[52]; Faure Walker et al.[57]). Compared to the Central Taurides, the upper crustal extension is better constrained in the Apennines due to the higher seismic activity and the surface-breaking earthquakes (such as the earthquakes of April 6, 2009 Mw 6.3 in L'Aquila, of August 24, 2016 Mw 6.2 in Amatrice and of October 30, 2016 Mw 6.6 in Norcia) (Cowie et al.[58]). In contrast, the Central Taurides today are characterized by shallow earthquakes usually not higher than Mw 4.5 (Güvercin et al.[18]; Aykut et al.[12]), and there is no historical and paleoseismological data on the faults. The difference in seismicity levels between two similar regions is not yet fully understood. The reduced seismic activity in the Central Taurides compared to the Apennines might be a combination of several factors, including lower tectonic stress (Cowie et al.[58]; Weiss et al.[59]) or the accommodation of significant stress by other structures (e.g. Western Anatolian Extensional Province, Ecemiş Fault, East Anatolian Fault) (Weiss et al.[59]). Because of lower strain, faults within the Central Taurides might have longer earthquake recurrence intervals and still need time to trigger seismic activity. For this reason, applying U-Th geochronology to syn-tectonic calcites, combined with kinematic and microstructural observations above the Cyprus Subduction Zone, significantly advances our understanding of upper plate evolution, where mantle-rooted processes control the surface deformation. This opens up a new window to constrain timing and mechanism of upper crustal modification and evaluate seismological hazard potential in such complex tectonic settings.

The Central Taurides represent a distinct geological and physiographical province within Anatolia, characterized by unique geomorphological features (e.g. tectono-karstic depressions) in a high-relief topography. The neotectonic provinces of Anatolia traditionally include regions such as the East Anatolian Contractional Province, the Central Anatolian Ova Province, the West Anatolian Extensional Province, and the North Turkish Province (Şengör et al. [60]). These provinces are defined based on their tectonic settings, deformation modes, and geological characteristics. However, the Taurides, the biggest mountain range in Türkiye, has not been included (except for the eastern Taurides) in this tectonic zonation scheme because of a lack of sufficient data to quantify the neotectonic activity of the faults within the mountain range. Our data do not cover all of the Taurides. Still, they reveal that the Central Taurides region stands out due to its specific neotectonic features, including upper crustal extension concurrent with rapid regional Quaternary uplift. Uplift and extension suggest a different geodynamic mechanism, possibly involving slab deformation and mantle upwelling, distinguishing it from other neotectonic provinces in Anatolia. Given the distinctiveness of the Central Taurides' neotectonic features and deformation mode, the "Central Taurides Neotectonic Extensional Province" is being proposed as a new sub-tectonic province within the neotectonic framework of Anatolia. This suggestion acknowledges the region's unique geological processes and aims to provide a more accurate classification that reflects Anatolia's specific tectonic characteristics and evolution.

https://doi.org/10.1038/s41467-024-55802-w

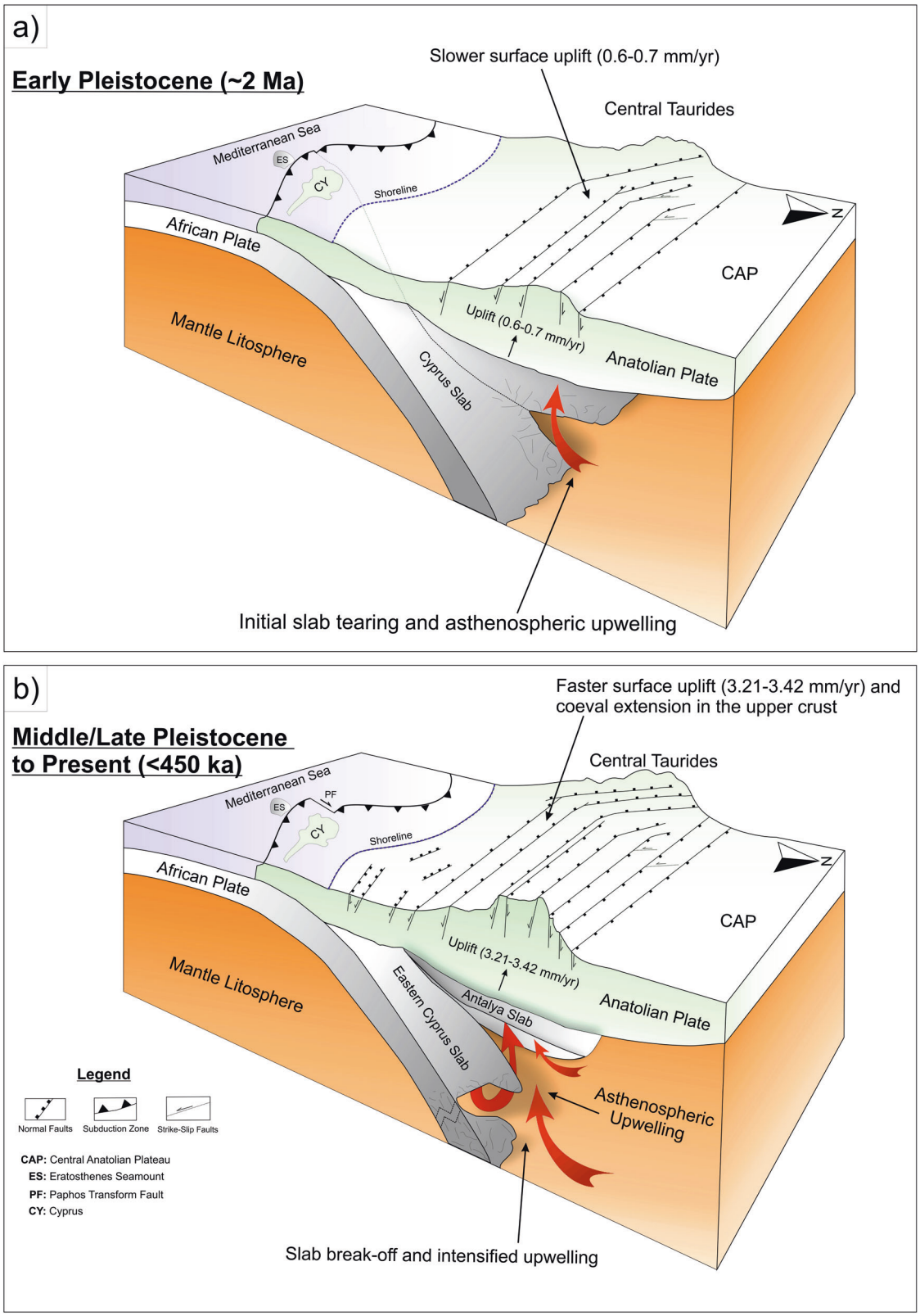

Fig. 7 | Conceptual diagram and interpretation of the relationships between deep-rooted processes and surface deformation in the Cyprus Subduction Zone from Early Pleistocene to Present. a Tectonic processes from ~2 Ma to 450 ka, illustrating the onset of slab deformation and asthenospheric upwelling beneath the overriding Anatolian Plate. **b** Tectonic processes from 450 ka to the present, showing the progression of the slab gap, intensification of mantle upwelling, and accelerated surface uplift and extensional deformation in the upper crust, leading to the current tectonic configuration in the Central Taurides. Please note that fault network and slab geometries are modified and simplified. Slab geometries are from Biryol et al.[4] and Portner et al.[9]. Surface uplift rates are from Schildgen et al.[6] and Öğretmen et al.[8].

In conclusion, our results, together with previous geomorphic, geophysical, biostratigraphic and geodynamic evidence, suggest that rapid surface uplift and extensional brittle deformation may occur concurrently, creating major relief-bounding normal fault zones and high-relief dynamic landscapes on a short timescale in the overriding plates (Fig. 7). Furthermore, the results of this study highlight the importance of U-Th geochronology of syn-tectonic carbonates, especially in erosional landscapes, for understanding the geodynamic evolution of convergent continental plates. Our methods and results have great potential for further studies on mantle-driven crustal deformation and the seismic hazard potential above the active plate boundaries.

Methods

Kinematic measurements and paleo-stress analysis

The kinematic measurements provide qualitative data for understanding the mechanism of brittle deformation and the sense of motion between fault blocks. Analysis of the fault-slip data enables us to establish principal paleo strain axes along the major fault zones (Delvaux and Sperner[61]; Karabacak et al.[38]). We obtained kinematic data from slickenlines and slicken fibres, which demonstrate the sense of motion between fault blocks. We used Win-Tensor software (Delvaux and Sperner[61]) to plot fault-slip data and determine extension and shortening directions. We plotted principal strain axes and interpreted the mode of the active upper crustal deformation. Because the displacements on the small-scale minor faults are small, we infer that no significant rotations occurred, hence the strain and stress axes are subparallel to each other. We infer that maximum and least compressive stress is parallel to shortening and extension directions, respectively. Details of the paleo-stress analysis are given in Table S1 in the supplementary file.

Microstructural analysis

Microstructural characteristics of fault-related calcite crystals provide important information on the relationships between crystal growth and faulting (Uysal et al.[33,34]; Nuriel et al.[36,37]; Karabacak et al.[38]). To investigate microstructural structures and textures, fault-related calcite crystals have been examined by optical and scanning electron microscope (SEM) analysis on thin sections. SEM analyses were conducted at the Nuclear Science Institute of Ankara University, utilizing ZEISS EVO 40 (500 V–30 kV). Petrographic microscope analysis was performed using James Swift (England) MP3500A polarizing microscope at the Department of Geological Engineering-Hacettepe University.

U-series (U-Th) carbonate geochronology

During seismically active periods, CO_2 degassing events and pressure solutions cause carbonate precipitation within crustal weakness zones such as fault planes (Uysal et al.[33,34]; Oren et al.[39]; Karabacak et al.[38]). These carbonates can form during syn-tectonic (calcite fibres, striated calcites, calcite cement), co-seismic (calcite gouge) and inter-seismic (carbonate coatings) periods (Nuriel et al.[37]). Syn-tectonic carbonate precipitates can be used to date the faulting events and are of great importance in paleoseismic and neotectonic studies (Nuriel et al.[36,37]; Uysal et al.[35]; Karabacak et al.[38]). For the application of U-Th carbonate geochronology, we conducted a syn-tectonic calcite sampling campaign across western Central Taurides, aimed at syn-tectonic calcite fabrics. We sampled and analysed twenty-six calcite fibres/striated calcites and two striated carbonate coatings along fault planes to constrain active brittle deformation. Details of U-Th geochronology data are given in Table S2, in supplementary file.

U-series dating was carried out using a Nu Plasma multi-collector inductively-coupled plasma mass spectrometer (MC-ICP-MS) in the Radiogenic Isotope Facility (RIF) at the School of the Environment, The University of Queensland (UQ) following chemical treatment procedures and MC-ICP-MS analytical protocols described elsewhere (Zhao et al.[62]; Clark et al.[63,64]). Powdered or chipped sub-samples weighing 3–170 mg were spiked with a mixed ^{229}Th-^{233}U tracer and then completely dissolved by drop-by-drop addition of concentrated HNO_3. After digestion, each sample was treated with H_2O_2 to decompose trace amounts of organic matters (if any) and to facilitate complete sample-tracer homogenization. U and Th were separated using conventional anion-exchange column chemistry using Bio-Rad AG 1-X8 resin. After stripping off the matrix from the column using double-distilled 7 N HNO_3 as eluent, 3 ml of a 2% HNO_3 solution mixed with trace amount of HF was used to elute both U and Th into a 3.5-ml pre-cleaned test tube, ready for MC-ICP-MS analyses, without the need for further drying down and re-mixing. After column chemistry, the U-Th mixed solution was injected into the MC-ICP-MS through a DSN-100 desolation nebuliser system with an uptake rate of around 0.1 ml per min. U-Th isotopic ratio measurement was performed on the MC-ICP-MS using a detector configuration to allow simultaneous measurements of both U and Th isotopes (Zhou et al.[65]; Clark et al.[64]). The ^{230}Th/^{238}U and ^{234}U/^{238}U activity ratios of the samples were calculated using the decay constants given in Cheng et al.[66] The non-radiogenic ^{230}Th was corrected using an assumed bulk-Earth atomic ^{230}Th/^{232}Th ratio of $4.4 \pm 2.2 \times 10^{-6}$. U-series ages were calculated using the Isoplot/Ex 3.75 Program (Ludwig[67]).

Data availability

All the data used in this study can be obtained in the figures, tables, references and the supplementary material

References

1. Faccenna, C., Bellier, O., Martinod, J., Piromallo, C. & Regard, V. Slab detachment beneath eastern Anatolia: a possible cause for the formation of the North Anatolian fault. *Earth Planet. Sci. Lett.* **242**, 85–97 (2006).
2. Schildgen, T. F., Yildirim, C., Cosentino, D. & Strecker, M. R. Linking slab breakoff, Hellenic trench retreat, and uplift of the Central and Eastern Anatolian Plateaus. *Earth-Sci. Rev.* **128**, 147–168 (2014).
3. Mutlu, A. K. & Karabulut, H. Anisotropic Pn tomography of Turkey and adjacent regions. *Geophys. J. Int.* **187**, 1743–1758 (2011).
4. Biryol, B. C., Beck, S. L., Zandt, G. & Özacar, A. A. Segmented African lithosphere beneath the Anatolian region inferred from teleseismic P-wave tomography. *Geophys. J. Int.* **184**, 1037–1057 (2011).
5. Cosentino, D. et al. Late Miocene surface uplift of the southern margin of the Central Anatolian Plateau, Central Taurides, Turkey. *Bull. Geol. Soc. Am.* **124**, 133–145 (2012).
6. Schildgen, T. F. et al. Multi-phased uplift of the southern margin of the Central Anatolian Plateau, Turkey: a record of tectonic and upper mantle processes. *Earth Planet. Sci. Lett.* **317–318**, 85–95 (2012a).
7. Schildgen, T. F. et al. Surface expression of eastern Mediterranean slab dynamics: Neogene topographic and structural evolution of the southwest margin of the Central Anatolian Plateau, Turkey. *Tectonics* **31**, TC2005 (2012b).
8. Öğretmen, N. et al. Evidence for 1.5 km of uplift of the Central Anatolian plateau's Southern Margin in the Last 450 kyr and implications for its multiphased uplift history. *Tectonics* **37**, 359–390 (2018).
9. Portner, D. E. et al. Subduction termination through progressive slab deformation across Eastern Mediterranean subduction zones from updated P-wave tomography beneath Anatolia. *Geosphere* **14**, 907–925 (2018).
10. Racano, S., Jara-Muñoz, J., Cosentino, D. & Melnick, D. Variable Quaternary Uplift Along the Southern Margin of the Central Anatolian Plateau Inferred from Modeling Marine Terrace Sequences. Tectonics 39 https://doi.org/10.1029/2019TC005921 (2020).

11. Racano, S., Schildgen, T. F., Cosentino, D. & Miller, S. R. Temporal and Spatial Variations in Rock Uplift from River-Profile Inversions at the Central Anatolian Plateau Southern Margin. *J. Geophys. Res.: Earth Surf.* **126**, 1–23 (2021).
12. Aykut, T., Yıldırım, C. & Uysal, I. T. Active Deformation Pattern in the Western Flank of the Central Taurides, Southern Margin of the Central Anatolian Plateau: inferences from geomorphic markers and kinematic indicators. *Tectonics*. **42**. https://doi.org/10.1029/2022TC007550 (2023).
13. Jolivet, L. & Faccenna, C. Mediterranean extension and the Africa-Eurasia collision. *Tectonics* **19**, 1095–1106 (2000).
14. Schattner, U. What triggered the early-to-mid Pleistocene tectonic transition across the entire eastern Mediterranean? *Earth Planet. Sci. Lett.* **289**, 539–548 (2010).
15. Ring, U., Glodny, J., Will, T. & Thomson, S. The hellenic subduction system: High-pressure metamorphism, exhumation, normal faulting, and large-scale extension. *Annu. Rev. Earth Planet. Sci.* **38**, 45–76 (2010).
16. Reilinger, R. et al. GPS constraints on continental deformation in the Africa-Arabia-Eurasia continental collision zone and implications for the dynamics of plate interactions. *J. Geophys. Res. Solid Earth*, **111**. https://doi.org/10.1029/2005JB004051 (2006).
17. Howell, A., Jackson, J., Copley, A., McKenzie, D. & Nissen, E. Subduction and vertical coastal motions in the eastern Mediterranean. *Geophys. J. Int.* **211**, 593–620 (2017).
18. Güvercin, S. E., Konca, A. Ö., Özbakır, A. D., Ergintav, S. & Karabulut, H. New focal mechanisms reveal fragmentation and active subduction of the Antalya slab in the Eastern Mediterranean. *Tectonophysics* **805**, 228792 (2021).
19. Wdowinski, S., Ben-Avraham, Z., Arvidsson, R. & Ekström, G. Seismotectonics of the Cyprian Arc. *Geophys. J. Int.* **164**, 176–181 (2006).
20. Imprescia, P., Pondrelli, S., Vannucci, G. & Gresta, S. Regional centroid moment tensor solutions in Cyprus from 1977 to the present and seismotectonic implications. *J. Seismol.* **16**, 147–167 (2012).
21. Robertson, A. H. F. Tectonic significance of the Eratosthenes Seamount: A continental fragment in the process of collision with a subduction zone in the Eastern Mediterranean (Ocean Drilling Program Leg 160). *Tectonophysics* **298**, 63–82 (1998).
22. Ring, U. & Pantazides, H. The uplift of the Troodos Massif, Cyprus. *Tectonics* **38**, 3124–3139 (2019).
23. Keskin, M. Magma generation by slab steepening and breakoff beneath a subduction-accretion complex: An alternative model for collision-related volcanism in Eastern Anatolia, Turkey. *Geophys. Res. Lett.* **30**, 7–10 (2003).
24. Şengör, A. M. C., Özeren, S., Genç, T. & Zor, E. East Anatolian High Plateau as a mantle-supported, north-south shortened domal structure. *Geophys. Res. Lett.* **30**, 8045 (2003).
25. Kinnaird, T. & Robertson, A. Tectonic and sedimentary response to subduction and incipient continental collision in southern cyprus, easternmost mediterranean region. *Geol. Soc. Spec. Publ.* **372**, 585–614 (2013).
26. Vernant, P., Reilinger, R. & McClusky, S. Geodetic evidence for low coupling on the Hellenic subduction plate interface. *Earth Planet. Sci. Lett.* **385**, 122–129 (2014).
27. Monod, O., Kuzucuoğlu, C. & Okay, A. I. A miocene palaeovalley network in the western Taurus (Turkey). *Turk. J. Earth Sci.* **15**, 1–23 (2006).
28. Kelletat, D. & Kayan, İ. Alanya batısındaki kıyılarda ilk C14 tarihlendirmelerinin ışığında Geç Holosen tektonik hareketleri. *TJK Bül.* **26**, 83–87 (1983).
29. Cosentino, D. et al. Evidence for latest Pleistocene to Holocene Uplift at the Southern Margin of the Central Anatolian Plateau (CAP), Southern Turkey. *EGU Gen. Assem.* **18**, 17–22 (2016).
30. Liberatore, M. et al. Vertical velocity fields along the Eastern Mediterranean coast as revealed by late Holocene sea-level markers. *Earth Sci. Rev.* **234**, 104199 (2022).
31. Şenel, M. 1/500.000 ölçekli Türkiye jeoloji haritası, Konya paftası. (MTA, 2002).
32. McPhee, P. J., Koç, A. & van Hinsbergen, D. J. J. Preparing the ground for plateau growth: late Neogene Central Anatolian uplift in the context of orogenic and geodynamic evolution since the Cretaceous. *Tectonophysics* **822**, 229131 (2022).
33. Uysal, I. T. et al. U-series dating and geochemical tracing of late Quaternary travertine in co-seismic fissures. *Earth Planet. Sci. Lett.* **257**, 450–462 (2007).
34. Uysal, I. T. et al. Hydrothermal CO2 degassing in seismically active zones during the late Quaternary. *Chem. Geol.* **265**, 442–454 (2009).
35. Uysal, I. T. et al. Linking CO_2 degassing in active fault zones to long-term changes in water balance and surface water circulation, an example from SW Turkey. *Quat. Sci. Rev.* **214**, 164–177 (2019).
36. Nuriel, P. et al. Formation of fault-related calcite precipitates and their implications for dating fault activity in the east Anatolian and dead sea fault zones. *Geol. Soc. Spec. Publ.* **359**, 229–248 (2011).
37. Nuriel, P. et al. U-Th dating of striated fault planes. *Geology* **40**, 647–650 (2012).
38. Karabacak, V., Sançar, T., Yildirim, G. & Uysal, I. T. When did the North Anatolian fault reach southern Marmara, Turkey? *Geology* **50**, 432–436 (2022).
39. Oren, O., Nuriel, P., Kylander-Clark, A. R. C. & Haviv, I. Evolution and propagation of an active plate boundary: U-Pb ages of fault-related calcite from the dead sea transform. *Tectonics* **39**, 1–14 (2020).
40. Fernández-Blanco, D., Mannu, U., Bertotti, G. & Willett, S. D. Forearc high uplift by lower crustal flow during growth of the Cyprus-Anatolian margin. *Earth Planet. Sci. Lett.* **544**, 116314 (2020).
41. Koç, A., Kaymakci, N., van Hinsbergen, D. J. J. & Vissers, R. L. M. A Miocene onset of the modern extensional regime in the Isparta angle: constraints from the Yalvaç Basin (Southwest Turkey). *Int. J. Earth Sci.* **105**, 369–398 (2016).
42. Koç, A., Kaymakci, N., Van Hinsbergen, D. J. J. & Kuiper, K. F. Miocene tectonic history of the Central Tauride intramontane basins, and the paleogeographic evolution of the Central Anatolian Plateau. *Glob. Planet. Chang.* **158**, 83–102 (2017).
43. Bartol, J. & Govers, R. A single cause for uplift of the Central and Eastern Anatolian plateau? *Tectonophysics* **637**, 116–136 (2014).
44. Meijers, M. J. M. et al. Rapid late Miocene surface uplift of the Central Anatolian Plateau margin. *Earth Planet. Sci. Lett.* **497**, 29–41 (2018).
45. Glover, C. P. & Robertson, A. H. F. Neotectonic intersection of the Aegean and Cyprus tectonic arcs: extensional and strike-slip faulting in the Isparta Angle, SW Turkey. *Tectonophysics* **298**, 103–132 (1998a).
46. Glover, C. P. & Robertson, A. H. F. Role of regional extension and uplift in the Plio-Pleistocene evolution of the Aksu Basin, SW Turkey. *J. Geol. Soc.* **155**, 365–387 (1998b).
47. van Hunen, J. & Allen, M. B. Continental collision and slab break-off: a comparison of 3-D numerical models with observations. *Earth Planet. Sci. Lett.* **302**, 27–37 (2011).
48. Duretz, T. & Gerya, T. V. Slab detachment during continental collision: influence of crustal rheology and interaction with lithospheric delamination. *Tectonophysics* **602**, 124–140 (2013).
49. Kiraly, A. et al. The effect of slab gaps on subduction dynamics and mantle upwelling. *Tectonophysics* **785**, 228458 (2020).
50. Koç, A., Kaymakci, N., van Hinsbergen, D. J. J., Kuiper, K. F. & Vissers, R. L. M. Tectono-Sedimentary evolution and geochronology of the Middle Miocene Altınapa Basin, and implications for the late Cenozoic uplift history of the Taurides, southern Turkey. *Tectonophysics* **532–535**, 134–155 (2012).

51. Çiner, A., Karabiyikoğlu, M., Monod, O., Deynoux, M. & Tuzcu, S. Late Cenozoic sedimentary evolution of the Antalya Basin, southern Turkey. *Turk. J. Earth Sci.* **17**, 1–41 (2008).
52. D'Agostino, N., Jackson, J. A., Dramis, F. & Funiciello, R. Interactions between mantle upwelling, drainage evolution and active normal faulting: an example from the Central Apennines (Italy). *Geophys. J. Int.* **147**, 475–497 (2001).
53. Blisniuk, P. M. et al. Normal faulting in central Tibet since at least 13.5 Myr ago. *Nature* **412**, 628–632 (2001).
54. Li, Z., Qiu, J. S. & Yang, X. M. A review of the geochronology and geochemistry of late Yanshanian (Cretaceous) plutons along the Fujian coastal area of southeastern China: implications for magma evolution related to slab break-off and rollback in the cretaceous. *Earth-Sci. Rev.* **128**, 232–248 (2014).
55. Kar, N. et al. Rapid regional surface uplift of the northern Altiplano plateau revealed by multiproxy paleoclimate reconstruction. *Earth Planet. Sci. Lett.* **447**, 33–47 (2016).
56. Nocquet, J. M. et al. Present-day uplift of the western Alps. *Sci. Rep.* **6**, 28404 (2016).
57. Faure Walker, J. P. et al. Relationship between topography, rates of extension and mantle dynamics in the actively extending Italian Apennines. *Earth Planet. Sci. Lett.* **325–326**, 76–84 (2012).
58. Cowie, P. et al. Orogen-scale uplift in the central Italian Apennines drives episodic behaviour of earthquake faults. *Sci. Rep.* **7**, 44858 (2017).
59. Weiss, J. R. et al. High-resolution surface velocities and strain for Anatolia from Sentinel-1 InSAR and GNSS data. *Geophy. Res. Lett.* **47**, e2020GL087376 (2020).
60. Şengör, A. M. C., Görür, N. & Şaroğlu, F. Strike-slip deformation basin formation and sedimentation: Strike-slip faulting and related basin formation in zones of tectonic escape: Turkey as a case study. In *Strike-Slip Faulting and Basin Formation*. Vol. 37 (eds Biddle, K. T. & Christie-Blick, N.) 227–264 (Society of Economic Paleontologists and Mineralogist, Special Publication, 1985).
61. Delvaux, D. & Sperner, B. *New aspects of tectonic stress inversion with reference to the TENSOR program*. 75–100. http://citeseerx.ist.psu.edu/viewdoc/download?doi=10.1.1.728.5720&rep=rep1&type=pdf (Geological Society, London, Special Publications, 2003).
62. Zhao, J. X., Yu, K. F. & Feng, Y. X. High-precision 238U-234U-230Th disequilibrium dating of the recent past – a review. *Quat. Geochronol.* **4**, 423–433 (2009).
63. Clark, T. R. et al. Spatial variability of initial 230Th/232Th in modern Porites from the inshore region of the Great Barrier Reef. *Geochim. et. Cosmochim. Acta* **78**, 99–118 (2012).
64. Clark, T. R. et al. Discerning the timing and cause of historical mortality events in modern Porites from the Great Barrier Reef. *Geochim. et. Cosmochim. Acta* **138**, 57–80 (2014).
65. Zhou, H., Zhao, J., Qing, W., Feng, Y. & Tang, J. Speleothem-derived Asian summer monsoon variations in central China, 54-46 ka. *J. Quat. Sci.* **26**, 781–790 (2011).
66. Cheng, H. et al. The half-lives of uranium-234 and thorium-230. *Chem. Geol.* **169**, 17–33 (2000).
67. Ludwig, K. R. User's manual for Isoplot/Ex version 3.75: a geochronological toolkit for microsoft excel. *Berkeley Geochronol. Cent. Spec. Publ.* **5**, 75 (2012).
68. Tezel, T., Shibutani, T. & Kaypak, B. Crustal thickness of Turkey determined by receiver function. *J. Asian Earth Sci.* **75**, 36–45 (2013).
69. Chiba, T., Kaneta, S. & Suzuki, Y. Red relief image map: new visualization method for three dimensional data. in the international archives of the photogrammetry, remote sensing and spatial. *Inf. Sci.* **37**, 1071–1076 (2008).
70. Vermeesch, P. On the visualisation of detrital age distributions. *Chem. Geol.* **312–313**, 190–194 (2012).

Acknowledgements

This study was funded by the Scientific and Technological Research Council of Türkiye (TUBITAK) within the "2232 International Fellowship for Outstanding Researchers Program" (Grant No: 118C275 to I.T.U). This study also was supported by the Scientific and Technological Research Council of Türkiye's "2214-A International Research Fellowship Programme for PhD Students" (Grant No: 1059B142200520 to T.A.) and the Scientific Research Projects Department of Istanbul Technical University (Project No: TDKB-2024-45553 to C.Y. and T.A.). We thank Gökhan Yıldırım for his support in microstructural analysis. We would like to thank Douwe J. J. van Hinsbergen and Derya Gürer for their constructive comments, which improved an earlier version of the manuscript. We also would like to thank Taylor F. Schildgen and Nasim Mozafari for their thorough and constructive reviews, which improved the quality of the paper.

Author contributions

I.T.U designed the study and took the lead on fieldwork, data analysis and manuscript writing. T.A. and C.Y. developed the hypothesis, conceived the study, participated in the fieldwork, and wrote the manuscript with the contribution of I.T.U. U.R. participated in the fieldwork, contributed to the structural geological work, reviewed and edited the final manuscript. J-X.Z. was responsible for the high-quality U-Th analysis, reviewed and edited the final manuscript.

Competing interests

The authors declare no competing interests.

Additional information

Supplementary information The online version contains supplementary material available at https://doi.org/10.1038/s41467-024-55802-w.

Correspondence and requests for materials should be addressed to Tunahan Aykut or I. Tonguç. Uysal.

Peer review information *Nature Communications* thanks Nasim Mozafari Amiri, and the other, anonymous, reviewers for their contribution to the peer review of this work. A peer review file is available.

Reprints and permissions information is available at http://www.nature.com/reprints

Publisher's note Springer Nature remains neutral with regard to jurisdictional claims in published maps and institutional affiliations.

Open Access This article is licensed under a Creative Commons Attribution-NonCommercial-NoDerivatives 4.0 International License, which permits any non-commercial use, sharing, distribution and reproduction in any medium or format, as long as you give appropriate credit to the original author(s) and the source, provide a link to the Creative Commons licence, and indicate if you modified the licensed material. You do not have permission under this licence to share adapted material derived from this article or parts of it. The images or other third party material in this article are included in the article's Creative Commons licence, unless indicated otherwise in a credit line to the material. If material is not included in the article's Creative Commons licence and your intended use is not permitted by statutory regulation or exceeds the permitted use, you will need to obtain permission directly from the copyright holder. To view a copy of this licence, visit http://creativecommons.org/licenses/by-nc-nd/4.0/.

© The Author(s) 2025